

## **NUMERICAL MODELLING AND VALIDATION OF PRECIPITATION KINETICS IN ADVANCED CREEP RESISTANT AUSTENITIC STEEL**

**VUJIC STOJAN<sup>1</sup>, FAROOQ MUHAMMAD<sup>2</sup>, SONDEREGGER BERNHARD<sup>1</sup>, SANDSTRÖM ROLF<sup>2</sup>, SOMMITSCH CHRISTOF<sup>1</sup>**

<sup>1</sup> *Institute for Materials Science and Welding, Graz University of Technology,  
Kopernikusgasse 24, A-8010 Graz, Austria*

<sup>2</sup> *Department of Materials Science and Engineering, KTH,  
Brinellvägen 23, S-100 44 Stockholm, Sweden*

\*Corresponding author: stojan.vujic@tugraz.at

### **Abstract**

The austenitic steel Sanicro 25 is one of the most promising austenitic steels for the application in superheater tubes in coal fired thermal power plants. In this work, the microstructural evolution of this material during heat treatment and thermal ageing has been investigated. The investigations were carried out by light microscopy (LOM), scanning electron microscopy (SEM), transmission electron microscopy (TEM) and energy dispersive spectroscopy (EDS). Scheil calculations were carried out by thermo-kinetic software MatCalc to analyse the solidification process which indicates Nb(C,N), Cr<sub>2</sub>N and Laves phase in the melt. Long term precipitation calculations predict the formation of five precipitate types in Sanicro 25: M<sub>23</sub>C<sub>6</sub>, Z-phase, Nb(C,N), Laves and Cr<sub>2</sub>N. Phase fractions and mean radii evolution of precipitates were calculated and compared to the experimental results. Calculated precipitate evolution shows good compliance with experimental data.

**Key words:** Sanicro 25, austenitic steel, M<sub>23</sub>C<sub>6</sub>, Z-Phase, Nb(C,N), Laves, Cr<sub>2</sub>N, MatCalc

### **1. INTRODUCTION**

The increasing demand on electrical energy in Europe and the world can be met by a number of strategies; one of them is the increase of the efficiency of coal fired thermal power plants. Currently, the worlds' mean efficiency of coal fired power plants is approximately 30%, in Germany an efficiency of 38% is reached. This higher level is achieved by steam temperatures of 600°C and steam pressures of 285bar. An increase of the steam state to 700°C/350 bar will increase the efficiency up to 50% (Aschenbrenner, 2008). Materials for these

demanding conditions are austenitic steels such as Sanicro 25, HR3C or DMV310.

This work focusses on the material Sanicro 25, since only few data on the microstructural evolution during heat treatment and under creep loading and ageing conditions are available. Rautio and Bruce (2004) report about Nb-rich precipitates and small needle-shaped M<sub>23</sub>C<sub>6</sub> precipitates in Sanicro 25 aged at 700°C for 1000 h and 3000 h. M<sub>23</sub>C<sub>6</sub> were found inside grains and grain boundaries. Höglberg et al. (2010) write about nano-sized M<sub>23</sub>C<sub>6</sub> and Laves phases (identified by electron diffraction) in creep loaded specimens at 700°C, 210 MPa and a rupture time of 3153 h.

However, the evaluation of these materials requires extensive investigations. In this paper the investigations (SEM, TEM, phase fraction determination) of long aged (up to 10000 h at 700°C) samples were presented. Additionally, these experimental investigations are complemented by equilibrium - Scheil - and precipitation kinetic calculations carried out with the software package MatCalc (Svoboda et al., 2004; Kozeschnik et al., 2004a; Kozeschnik et al., 2004b).

## 2. EXPERIMENTAL

The microstructure investigations were performed on as-received and thermally aged tubes ( $\varnothing 38 \times 8$  mm) and plates (10x10x2 mm). The chemical compositions of all samples are presented in table 1.

**Table 1.** Chemical composition (weight %) Sanicro 25.

	C	Si	Mn	P	S	Cr	Ni	W	Co	Cu	Al	Nb	N	O
Tube	0.067	0.19	0.53	0.019	0.0008	22.21	24.55	3.35	1.49	2.89	0.038	0.51	0.23	-
Plate	0.0646	0.15	0.5	0.015	0.0005	22.6	25.4	3.7	1.5	2.9	0.062	0.48	0.2317	0.0165

Tube samples were solution annealed at 1220°C, plate samples at 1200°C; both sample types were quenched after annealing. This sample status is denoted as "as received" in the following.

After this heat treatment, a number of samples were thermally aged at 700°C; for details see table 2.

**Table 2.** Heat treatments of Sanicro 25.

Sample	Temperature / °C	Time / h
Tube	700	5000
Plate	700	1000
Plate	700	3000
Plate	700	10000

For the microstructure characterization, SEM (precipitates), TEM (precipitates) as well as LOM investigations (grain size) have been performed. The chemical compositions of precipitates were determined by EDS. The error for the determination of light elements (like C, N) is approximately  $\pm 10\%$  and error for the determination of heavy elements (like Cr, Nb, Ni, W) is approximately  $\pm 2-5\%$ .

All SEM and LOM samples were embedded, grinded, polished and afterwards etched. Etching of Sanicro 25 tube samples were performed by

Glyceregia (3 parts glycerine + 3 parts HCl + 1 part  $\text{HNO}_3$ ). Plate specimens for SEM were etched by electrolytic etching in a 10% solution of oxalic acid in distilled water at 3 Volt for 10 to 60 s, whereas plate specimens for TEM carbon replicas were etched with a solution of 40% HCl and 20%  $\text{HNO}_3$  in distilled water at 60°C for 10 s.

Thermodynamic calculations have been carried out with the thermo-kinetic software MatCalc (version 5.50) including the iron database (version 1.019). Equilibrium calculations give a picture of sample states after long ageing times, Scheil calculations indicate the formation of precipitates during the solidification processes and precipitate kinetic calculations indicate the nucleation, growth and coarsening processes during heat treatment and ageing.

## 3. RESULTS

### 3.1. As-received

In the as-received tube samples, large primary Nb-rich precipitates were found on grain boundaries and inside the grains, as shown in figure 1(A). The evaluation of the area fraction was achieved by phase contrast imaging in SEM and evaluated by the Software Zeiss KS400. Results indicate an area fraction of 1.6% and mean diameter of 945 nm, respectively. The grain size of the as-received tube sample is 43  $\mu\text{m}$  and was determined by the intercept method.

As-received plate samples also show Nb-rich precipitates with approximately 1  $\mu\text{m}$  mean diameter. Additional TEM investigations of as-received plate samples reveal secondary Nb(C,N) precipitates, see figure 1(B). EDS analysis of Nb(C,N) indicate a composition (wt%) of 54%Nb-30%Cr-0.6%C-2%N for precipitate 1, 51Nb-30Cr-0.8C-3N for precipitate 2 and 33Nb-22Cr-3.2C-5N for precipitate 3 in figure 1(B).

Table 3 indicates upper and lower limits for the composition of the primary Nb-rich precipitates in as-received plate specimens determined by EDS.



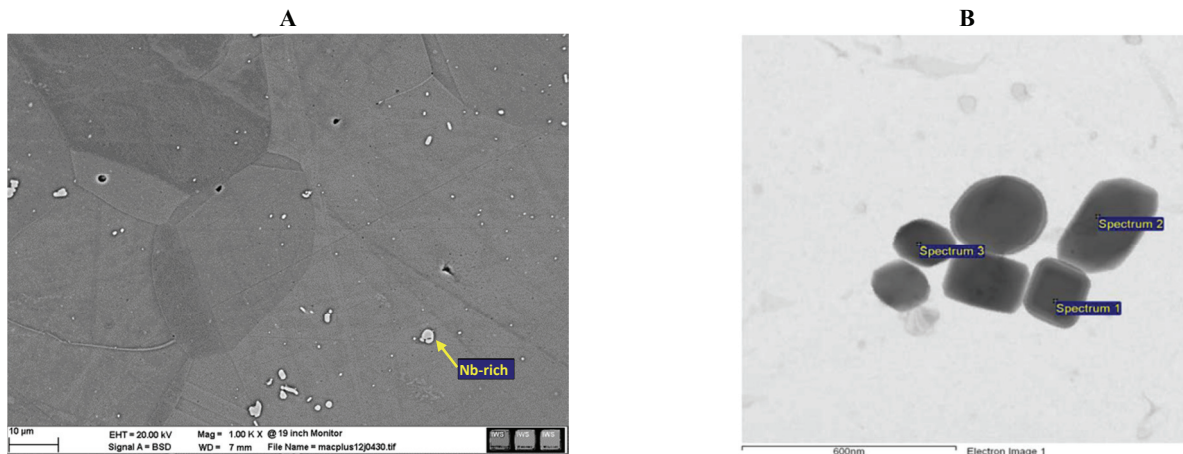


**Fig. 1.** SEM image of tube sample (A) and TEM image of plate sample (B) in Sanicro 25 in as-received condition.

**Table 3.** Composition (wt%) of Nb-rich phase in as-received Sanicro 25 by SEM.

	Cr		Nb		Ni		Si	
	Cr <sub>min</sub>	Cr <sub>max</sub>	Nb <sub>min</sub>	Nb <sub>max</sub>	Ni <sub>min</sub>	Ni <sub>max</sub>	Si <sub>min</sub>	Si <sub>max</sub>
As-received	24	29.5	11.6	60.5	1.2	19.4	0.1	0.1

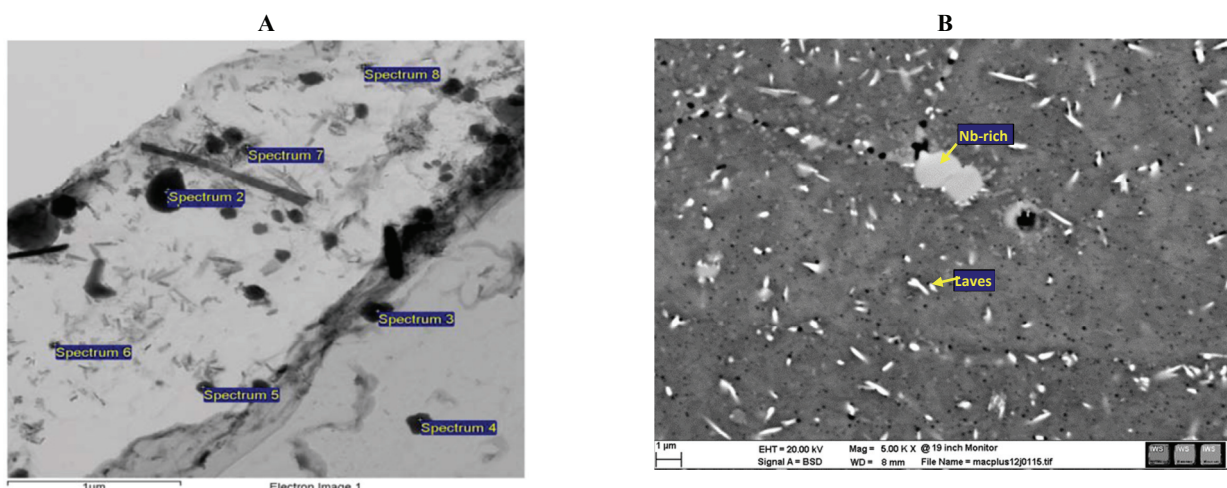


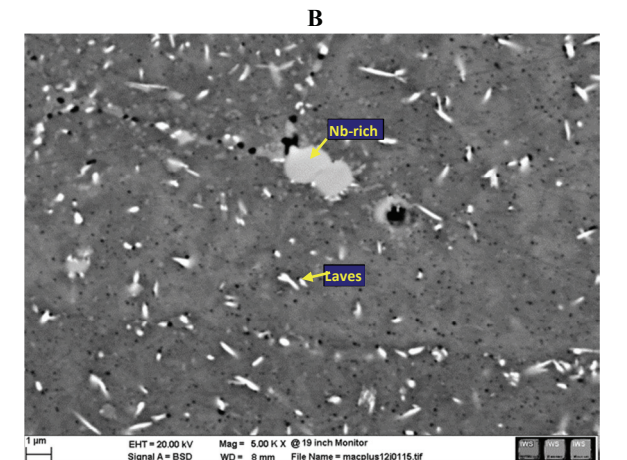
**Fig. 2.** TEM image of 700°C/1000 h plate sample (A) and SEM image of 700°C/5000 h tube sample (B).

### 3.2. Samples heat treated at 700°C

Plate samples aged at 700°C for 1000 h reveal six different precipitate types: primary Nb-rich, Cr<sub>2</sub>N, M<sub>23</sub>C<sub>6</sub>, Nb(C,N), Laves and oxides. Exemplarily, fig. 2(A) presents one of the TEM images of sample condition 700°C/1000 h taken from a carbon replica of a plate sample. Precipitates 2, 3, 4, 5 and 7 were identified by EDS as chromium-rich carbides, whereas precipitate 6 was identified as Nb(C,N) and precipitate 8 as niobium chromium carbide. Figure 2(B) indicates a representative SEM image of a 700°C/5000 h tube

sample, where large Nb-rich precipitates and bright W-rich Laves phase can be observed.

The microstructure of plate samples aged for 10000 h at 700°C is exemplarily shown in figure 3(A) (SEM image). Precipitate 1, 2, 4 were identified as Nb-rich and 3, 5, 6 as Cr<sub>2</sub>N. TEM investigations of the same sample reveal four different precipitate types: Laves, M<sub>23</sub>C<sub>6</sub>, Nb(C,N) and Si-oxides;



Si-oxide (precipitate 2, 3) and M<sub>23</sub>C<sub>6</sub> (precipitate 1) are presented in figure 3(B).

The TEM investigations of different phases for 700°C at different aging times are summarized in table 4.

In the present paper the focus is on the precipitation of fine particles (<0.25 μm). Coarser particles of Z-phase (>0.5 μm) are also observed after long term ageing, but they are not analysed.

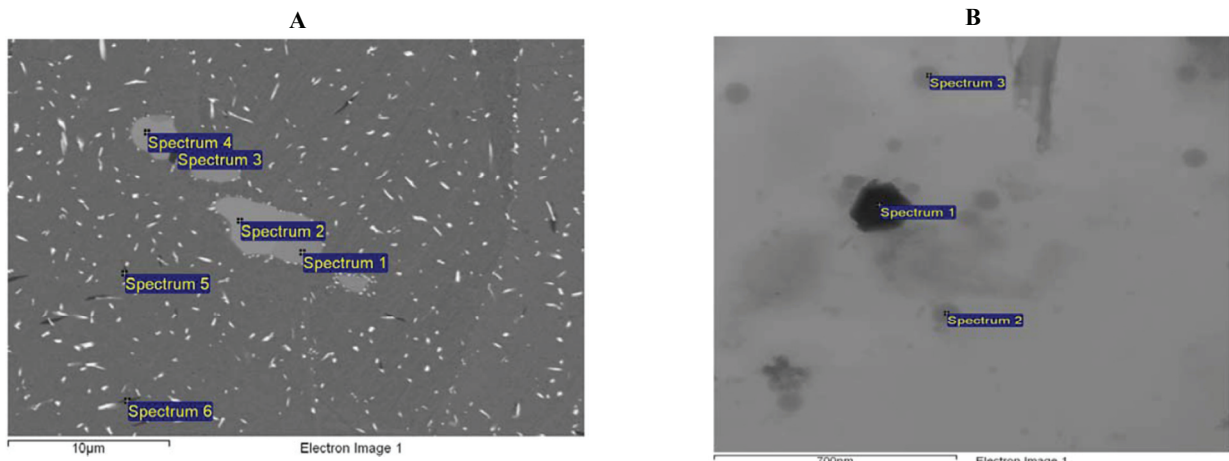


**Fig. 3.** SEM image (A) and TEM image (B) of 700°C/10000h plate sample.

**Table 4.** Composition (wt%) of different phases in Sanicro 25 plate samples aged at 700°C.

Aging Time hours	Aging Temp. °C	Phase	Cr		Nb		Ni		C		N		W	
			Cr <sub>min</sub>	Cr <sub>max</sub>	Nb <sub>min</sub>	Nb <sub>max</sub>	Ni <sub>min</sub>	Ni <sub>max</sub>	C <sub>min</sub>	C <sub>max</sub>	N <sub>min</sub>	N <sub>max</sub>	W <sub>min</sub>	W <sub>max</sub>
As received	As received	Nb(C,N)	23.1	32.4	35.9	55.6	0.2	1.4	0.12	3.16	1.4	5.7	3.1	6.1
1000	700	Cr <sub>2</sub> N	57.7	66	3.5	13.2	1.8	2.9	0.69	0.99	1.2	2.6	8.6	9.1
1000	700	Nb(C,N)	13	40.9	13.7	67.6	0	0.9	0.77	6.58	0	5.1	0	2.9
10000	700	M <sub>23</sub> C <sub>6</sub>	56.2	89	0	6.1	0.1	6.1	0.62	1.54	0	0.8	0	10.8
10000	700	Laves	10.3	17.9	0	5.7	1.2	2	-	-	-	-	40.1	59.6
10000	700	M <sub>23</sub> C <sub>6</sub>	47.7	67.9	0	4.7	1.8	2.7	0.96	3.39	-	-	8.6	13.4
10000	700	Nb(C,N)	17.9	30.1	22.9	36.7	0	0.2	3.24	5.35	0	1.0	1.1	2.8

### 3.3. Calculation of microstructure by MatCalc

#### 3.3.1. Equilibrium and Scheil calculation

Within the considered temperature regime of 500-1450°C, MatCalc predicts the stability of nine different equilibrium phases: liquid and austenite as matrix phase respectively, Nb(C,N), Cr<sub>2</sub>N, Cu, Laves, sigma, M<sub>23</sub>C<sub>6</sub> and Z-phase as stable precipitate phase; see figure 4(A). Nb(C,N) shows a stable temperature regime between 1150-1350°C, Cr<sub>2</sub>N is stable below 1325°C, Cu-phase and Laves phase up to 900°C. Sigma phase is only stable up to 730°C. For the temperature dependent phase fractions, see figure 4(A). All results show good agreement to the experimental data, except for the Cr<sub>2</sub>N: The measured phase fraction after long term ageing, which should indicate equilibrium, was found significantly lower compared to the equilibrium calculations. For this reason, the Gibbs free energy of Cr<sub>2</sub>N was increased by 450 J in order to adapt the thermodynamic database to the present system.

Scheil-calculations (Kozeneschnik, 2010) were performed to investigate the effect of segregation processes during solidification on the formation of the precipitates. For the calculation, only back-diffusion of C and N was allowed, all other elements were assumed not diffusing during cooling. These conditions meet the situation for a broad bandwidth of medium cooling rates. It can be seen that in the Scheil calculation liquid phase keeps stable down to appr. 1240°C (1% phase fraction), which is more than 80°C lower compared to equilibrium. This phenomenon can be accorded to massive segregation in the liquid phase during the solidification process: calculations indicate a composition of the remaining melt (1%) of: 21.1Fe, 18.7Cr, 17.9Ni, 18.5Cu, 20.6W, 1.5Mn, 1.5Co, 0.1N, 0.05C (wt%). Equilibrium calculations of this remaining melt indicate a solidus temperature as low as 1240°C, so the lower liquidus temperature within the Scheil calculations is reasonable. During solidification, one matrix and three precipitate phases form: austenite, Nb(C,N), Cr<sub>2</sub>N and Laves phase, see figure 4(B).

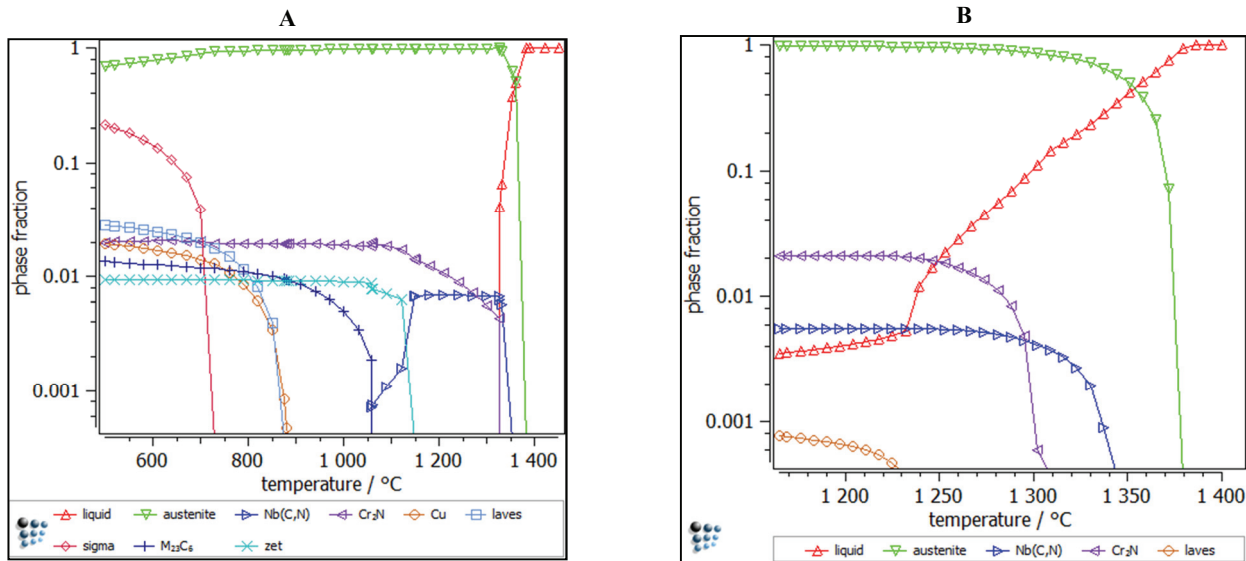


Fig. 4. Equilibrium (A) and Scheil (B) calculation of Sanicro 25.

### 3.3.2. Set up of precipitation calculation

Since precipitation kinetic simulations are generally restricted to the formation of particles due to diffusional processes in solid materials, primarily formed precipitates have to be considered separately. For this reason, the measured data on the primarily formed Nb-rich particles have to be used as input data. These precipitates withdraw Nb and other elements from the liquid during their formation. All kinetic calculations shown in the following have therefore been carried out as “system without primary Nb-particles” and accordingly corrected overall composition. The simulation of oxides has not been carried out due to the lack of oxygen within the thermodynamic database.

For the calculation, the grain size was defined as 43 $\mu\text{m}$ , the dislocation density was set at  $10^{12} \text{ m}^{-2}$ , which is typical for a well annealed austenitic steels (Kozeschnik, 2012). The dislocation core diffusivity was defined as  $10^{(7-0.0025\cdot T)}$  (T in K) and the grain boundary diffusivity as  $10^{(11-0.005\cdot T)}$  (T in K) which was recommended for Fe-austenitic steels (Radis & Kozeschnik, 2010). The temperature-dependence of Young's modulus for austenitic steels is defined as  $(210000-75\cdot T)\cdot 10^6$  (T in K).

Dislocations as nucleation sites were defined for all precipitates. Additionally, grain boundaries were nucleation sites for  $\text{M}_{23}\text{C}_6$ , Sigma, Cu, AlN, Laves,  $\text{Cr}_2\text{N}$  and subgrain boundaries for Z-phase and  $\text{Nb}(\text{C},\text{N})$ . The interfacial energies for the particles were calculated automatically by the GBB model (Sonderegger & Kozeschnik, 2009a). Each precipitate was calculated with interfacial energy size cor-

rection (Sonderegger & Kozeschnik, 2009b). Calculation of Laves phase was performed with diffuse interface correction (Sonderegger & Kozeschnik, 2010) due to the high ageing temperature of 700°C and the low solution temperature of this phase. On the basis of the investigations, it was assumed that the diffusion in the MatCalc database was too low. Therefore, the matrix diffusion enhancement for substitutional elements was defined as 15 for  $\text{M}_{23}\text{C}_6$ . The matrix diffusion enhancement for substitutional elements is 0.25 for  $\text{Cr}_2\text{N}$ .

For comparison with the experimental data, mean radii and phase fractions of the precipitates are the most convenient data. For the comparison it is necessary to convert the measured area fraction of the precipitates into phase fractions. This can be carried out by standard methods, indicated by equations (1-5).

$$f_i = \frac{n_i}{\sum_i n_i} \quad (1)$$

$$n_i = \frac{V_i}{V_{M,i}} \quad (2)$$

$$A_{A,i} = \frac{A_i}{\sum_i A_i} \quad (3)$$

$$\frac{V_i}{\sum_i V_i} = \frac{A_i}{\sum_i A_i} \quad (4)$$

$$f_i = \frac{\frac{A_{A,i}}{V_{M,i}}}{\sum_i \frac{A_{A,i}}{V_{M,i}}} \quad (5)$$

$f$  is the molar phase fraction,  $n$  number of moles of substance,  $A_A$  the area fraction,  $V$  the volume,  $V_M$  the molar volume and  $A$  the measured area of each phase. The phase fraction (5) can be calculated by inserting (2, 3, 4) into (1). Volume ratio (4) was

equated to area ratio due to the homogeneous distribution in the matrix, following the Cavalieri-Hacquet principle (Underwood, 1970). The molar volume for each phase was calculated by MatCalc.

### 3.3.3. Precipitation calculation at 700°C

The precipitation calculation at 700°C for 12000 h was performed after a solution annealing calculation at 1220°C/5 min. The calculation is predicting eight different precipitate types:  $M_{23}C_6$ , Z-phase, Nb(C,N), Laves, Cr<sub>2</sub>N, AlN, Cu-phase and sigma. Table 5 presents the chemical composition of calculated precipitates at 700°C for 10000 h, which is the longest ageing time.

**Table 5.** Composition (wt%) of the precipitates at 700°C after 10.000 h.

	C	N	Mn	Fe	Co	Cr	Ni	W	Nb
Laves	-	-	-	20.605	-	16.244	-	63.135	0.015
Cr <sub>2</sub> N	0.451	10.697	0.023	0.112	0.002	88.330	0.022	0.362	-
$M_{23}C_6$	5.220	-	0.076	4.838	0.070	78.532	0.448	10.817	-
Z-Phase	-	8.720	-	6.258	-	26.773	-	-	58.249
Nb(C,N)	0.279	14.276	-	-	-	15.685	-	0.040	69.720

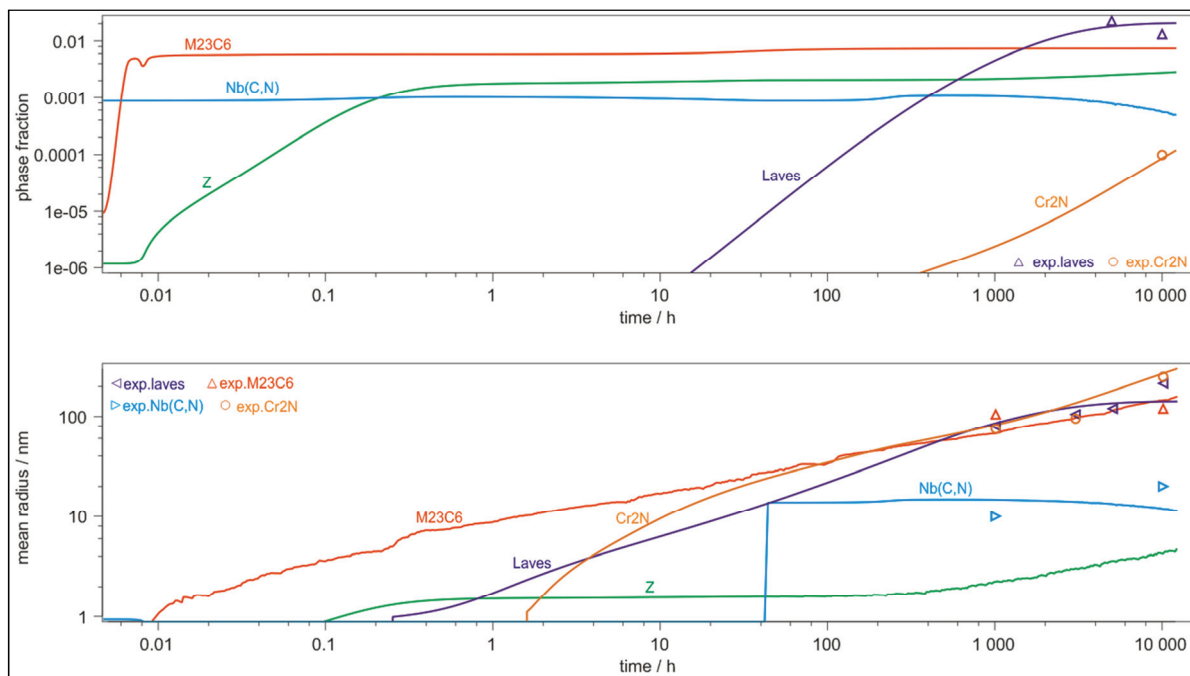


**Fig. 5.** Phase fractions and mean radii of precipitates in Sanicro 25 aged at 700°C for 12000 h.

Figure 5 presents the calculated results for phase fractions and particle radii plus a comparison with the experimentally found data. The phase fractions of AlN, Cu-phase, Sigma phase were smaller than  $10^{-7}$  and therefore not plotted.  $M_{23}C_6$  precipitates reach the equilibrium phase fraction of 0.7% after approximately 60 h and constant coarsening up to

mean radii of 120 nm at 10000 h. The phase fraction of secondary Z-phase is 0.2%. These precipitates also show extremely small mean radii of 1.5–4 nm. Secondary Nb(C,N) precipitates are the only precipitate type remaining during the solution treatment at 1220°C with a phase fraction of 0.1%. However, their radius turns out to be extremely small at the end of the solution treatment due to extensive nucleation during cooling. During ageing, their mean radii increase to 10 nm (1000 h) and 15 nm (10000 h), respectively. Laves phase shows a continuous increase of phase fraction up to 2% until the equilibrium is reached. Parallelly, their radii grow up to 150 nm.



Cr<sub>2</sub>N shows a slow increase of the phase fraction which is 0.01% after 10000 h aging time. At this ageing time, the particles are still in the growing stage reaching mean radii of 220 nm.

## 4. DISCUSSION

Large Nb-rich precipitates (average size  $1\mu\text{m}$ ) were found in as-received sample state. The large size of these precipitates suggests that these precipitates formed primarily during the solidification process. Equilibrium and Scheil calculations indicate that Nb(C,N) is present in the liquid range. Therefore, from the thermodynamic calculations alone, it could be concluded that this phase is Nb(C,N). On the other hand, measured chemical compositions (SEM) are closer to the typical composition of Z-phase. Since the scatter of compositions between individual precipitates is too large, no final conclusion can be drawn at this point. However, the question on the nature of these precipitates does not significantly affect the precipitate kinetic calculations, since the chemical composition of the remaining matrix can be adapted according to the measured compositions of the particles.

As concerns the secondary precipitates, the accordance of simulated and measured data is very good. Figure 5 indicates the experimentally found data and compares them to the simulation results. Precipitate radii are available for  $\text{M}_{23}\text{C}_6$ , Nb(C,N), laves phase and  $\text{Cr}_2\text{N}$ , volume fractions have been measured for Laves and  $\text{Cr}_2\text{N}$ . All these data are in very good agreement. The only deviations are found in the phase fraction and radii of secondary Z-phase particles; whereas simulations indicate particles of 1.5-4 nm in size, these precipitates have not been found by the experimental investigations. This might be explained by the very small radii of the particles, which makes the experimental investigation extremely difficult. A similar statement can be given about precipitate types AlN, Cu and sigma phase. Whereas these particles should form in principle, the calculated phase fractions (smaller than  $10^{-7}$ ) are way too low for experimental investigations.

## 5. SUMMARY

Microstructure investigations and thermodynamic calculations of austenitic steel Sanicro 25 were carried out for as received- and thermally aged samples. For the investigations SEM, TEM and LOM techniques were performed.

Seven different precipitate types were found experimentally in Sanicro 25: primary Nb-rich precipitates, Al- and Si-oxides and secondary Nb(C,N), Laves phase,  $\text{Cr}_2\text{N}$  and  $\text{M}_{23}\text{C}_6$ . Primarily formed precipitates have to be considered separately in the kinetic calculations by introducing an “effective”

system composition, subtracting these particles’ impact. When including this effect, the calculations show a very good agreement with the experimental results.

With this calculation a basis was created for the precipitation strength calculation in order to optimize the Sanicro25 by modifying the chemical composition and heat treatment.

**Acknowledgments.** This investigation was sponsored by the European Union (directorate-general for energy), within the project MACPLUS (ENER/FP7EN/249809/MACPLUS) in the framework of the Clean Coal Technologies.

## REFERENCES

- Aschenbrenner, N., 2008, *Kohlekraftwerk strebt 50 Prozent Wirkungsgrad*, available at: <http://www.innovations-report.de>
- Högberg, J., Guocai, C., Kjellström, P., Boström, M., Forsberg, U., Sandström, R., 2010, Creep behaviour of the newly developed advanced heat resistant austenitic stainless steel grade UNS S31035, *ASME Pressure Vessels And Piping Conference*, Bellevue, 421-428.
- Kozeneschnik, E., 2010, *Simulation of solidification of 0.7C 3Mn steel*, available at: <http://matcalc.tuwien.ac.at/>
- Kozeneschnik, E., 2012, *Diffusion in heterogeneous precipitation*, available at: <http://matcalc.tuwien.ac.at/>
- Kozeneschnik, E., Svoboda J., Fischer F.D., 2004a, Modified evolution equations for the precipitation kinetics of complex phases in multi-component systems, *Calphad*, 28, 379-382.
- Kozeneschnik, E., Svoboda, J., Fratzl, P., Fischer, F.D., 2004b, Modelling of kinetics in multi-component multi-phase systems with spherical precipitates: II: Numerical solution and application, *Materials Science and Engineering A*, 385, 157-165.
- Radis, R., Kozeneschnik, E., 2010, Kinetics of AlN precipitation in microalloyed steel, *Modelling and Simulation in Materials Science and Engineering*, 18, 055003.
- Rautio, R., Bruce, C., 2004, Sandvik Sanicro 25, A New Material for Ultrasupercritical Coal Fired Boilers, *ASM*, 274-290.
- Sonderegger B., Kozeneschnik E., 2009a, Generalized nearest neighbour broken-bond analysis of randomly oriented coherent interfaces in multicomponent fcc and bcc structures, *Metallurgical and Materials Transactions A*, 40, 499-510.
- Sonderegger B., Kozeneschnik E., 2009b, Size dependence of the interfacial energy in the generalized nearest-neighbor broken-bond approach, *Scripta Materialia*, 60, 635-638.
- Sonderegger B., Kozeneschnik E., 2010, Interfacial Energy of Diffuse Phase Boundaries in the Generalized Broken-Bond Approach, *Metallurgical and Materials Transactions A*, 41, 3262-3269.
- Svoboda J., Fischer F.D., Fratzl P., Kozeneschnik E., 2004a, Modelling of kinetics in multi-component multi-phase systems with spherical precipitates: I: Theory, *Materials Science and Engineering A*, 385, 166-174.



Underwood E. E., 1970, *Quantitative Stereology*, Addison-Wesley, 27.

**NUMERYCZNE MODELOWANIE I WERYFIKACJA  
KINETYKI WYDZIELEŃ W ZAAWANSOWANYCH  
STALACH AUSTENITYCZNYCH ODPORNYCH NA  
PEŁZANIE**

Streszczenie

Stal austenityczna Sanicro 25 jest jedną z obiecujących stali do zastosowań na rury w wymiennikach ciepła w elektrowniach węglowych. W niniejszej pracy przeprowadzono badania rozwoju mikrostruktury podczas obróbki cieplnej i sztucznego starzenia tych stali. Badania wykonano za pomocą mikroskopu optycznego (LOM), skaningowego mikroskopu elektronowego (SEM), elektronowego mikroskopu transmisyjnego (TEM) i spektroskopu (EDS). Obliczenia metodą Scheila przeprowadzono wykorzystując oprogramowanie MatCalc. Analizowano proces krzepnięcia, w którym powstają fazy Nb(C,N), Cr<sub>2</sub>N oraz faza Lavesa. Obliczenia długoterminowego procesu wydzielania wykazały, że w Sanicro 25 powstaje 5 różnych faz: M<sub>23</sub>C<sub>6</sub>, faza-Z, Nb(C,N), faza Lavesa oraz Cr<sub>2</sub>N. Obliczone ułamki objętości poszczególnych faz oraz średni promień rosnących wydzieleń zostały porównane z wynikami doświadczeń i otrzymano dobrą zgodność.

*Received: August 10, 2012*

*Received in a revised form: December 5, 2012*

*Accepted: December 20, 2012*

